Molecular Dynamics Modeling of Tubular Aluminum Silicate: Imogolite

Keiko Tamura* and Katsuyuki Kawamura

Department of Earth and Planetary Science, Tokyo Institute of Technology, Tokyo 152-8551, Japan

Received: June 29, 2001; In Final Form: October 16, 2001

The molecular models of tubular aluminumsilicate, imogolite, and tubular gibbsite for the comparison with imogolite were investigated by means of molecular dynamics simulations. The stability of these two models was tested in terms of the tube radii. It was shown that the total energy of tubular gibbsite is decreasing monotonically with the increasing radius of the tube. On the contrary, the total energy of imogolite has the minimum around diameter 2.6−2.9 nm. The details of the imogolite stability were inspected in terms of atom potential energy and the structural details.

1. Introduction

Imogolite is naturally occurring hydrous aluminumsilicate found in soils of volcanic origin and with an SiO_2/Al_2O_3 ratio of about 1.0. The structural model of imogolite was proposed by Cradwick et al.[1] from the electron diffraction observations. They concluded that the wall of the imogolite molecule is composed of a tubular gibbsite sheet and orthosilicate anions associate on each vacant octahedral sites of the gibbsite sheet. The Si−OH group that is one corner of an SiO_4 tetrahedron is pointing toward the inside of the tube and the other three O atoms are shared with octahedra of Al in the gibbsite sheet. This structure has a composition of $Al_2(OH)_3SiO_3OH$. The tubular structure of imogolite was explained by a shortening of O−O distances of vacant octahedral sites that arise from size misfit caused by bonding of orthosilicate anion with gibbsite sheet. Most of the studies reported afterward have been based on this structural model.

The synthesis of imogolite was reported by Farmer et al.[2,3] Proto-imogolite was formed by the interaction of hydroxyaluminum cations with orthosilicic acid in dilute solutions at pH less than about 5. Synthetic imogolite was formed by heating the solutions to 96−100 °C. It is shown by electron microscopy, electron diffraction, and X-ray diffraction that the tube diameter of synthetic imogolite is larger than that of natural imogolite. From X-ray diffraction patterns of films dried at 100 °C, they concluded that the center-to-center separation between tubes is 2.27 nm for natural and 2.62 nm for synthetic imogolite and that natural imogolite has a circumference composed of 12 gibbsite units and synthetic imogolite has 14 units. Wada et al. reported that the synthetic Ge-substituted imogolite that has 18 gibbsite units around the circumference of the tube.[4,5] Wada et al. synthesized imogolite at 25 °C by aging solutions containing monomeric silicic acid and polymeric hydroxyaluminum ions for 7 years.[6] The diameter of this imogolite was 2.3 ± 0.2 nm, which is closer to that of natural imogolite (2.1 ± 0.2 nm) than to that of imogolite synthesized at about 100 °C (2.8 ± 0.1 nm). These diameters were estimated from electron micrographs. Recently, Bursill et al. reported that the diameter of the imogolite tube was approximately 2.5 nm by means of high-resolution transmission electron microscopy.[7]

Imogolites have been studied over the years, due to their excellent properties in adsorption. In particular, they are characterized by their tubular structure, which is expected for a shape/size selective material.[8−12] The molecular simulation method is one of the most effective methods to treat systems that include a large number of atoms, from several hundreds to several tens of thousands, and this number of atoms is needed to model the systems containing imogolite structures. Much attention has been paid to adsorption on the surface of clay minerals, and studies that used computational simulation methods have been reported, where clays were described as fully or partially rigid models in the most of these studies.[13−16] Only a few simulations adopted an atomistic model.[17−21] We have found no computational studies of imogolite using atomistic models that can be used with the molecular dynamic method of total freedom of atom motions.[22−24] It is important to use the model that allows all motions of atoms including hydrogen when the purpose of simulation is to investigate the properties influenced by the dynamic behavior of atoms, for example, adsorption, surface diffusion, etc.

The purpose of this study is to establish a structural and an interatomic potential model of imogolite molecules that takes all degrees of freedom of atom motions into account. The tubular gibbsite molecular model, which has structural parts common to imogolite, was also set up to compare with imogolite. Molecular dynamics simulations were performed to investigate the stability of these molecules.

2. Simulation Method

Interatomic Potential Model. The interaction between atoms should be described relevantly to produce a precise molecular model.[25] In this study, the interatomic potential functions below were employed.

Two-body terms:

$$u_{ij}(r_{ij}) = \frac{z_i z_j e^2}{4\pi\epsilon_0 r_{ij}} + f_0(b_i + b_j)\exp\left[\frac{a_i + a_j - r_{ij}}{b_i + b_j}\right] - \frac{c_i c_j}{r_{ij}^6} + D_{1ij}\exp(-\beta_{1ij} r_{ij}) + D_{2ij}\exp(-\beta_{2ij} r_{ij}) + D_{3ij}\exp[-\beta_{3ij}(r_{ij} - r_{ij}^*)^2]$$

Three-body terms:

$$u_{jik}(r_{ij}, r_{ik}, \theta_{jik}) = -f_k[\cos\{2(\theta_{jik} - \theta_0)\} - 1]\sqrt{k_j k_k}$$

$$k_j = 1/[\exp\{g_r(r_{ij} - r_m)\} + 1]$$

* To whom correspondence should be addressed. E-mail: k-tamura@geo.titech.ac.jp. Phone: +81-3-5734-2616. Fax:+81-3-5734-3538

10.1021/jp0124793 CCC: $22.00
Published on Web 12/13/2001

TABLE 1: Interatomic Parameters Used in the MD Simulations (a) for Tubular Gibbsite and (b) for Imogolite

(a) Gibbsite

	O atom	Al atom	H atom
z/e	−1.100	1.800	0.500
w/10^{-3} kg mol^{-1}	16.00	26.98	1.01
a/nm	0.1876	0.1030	0.0100
b/nm	0.0150	0.0080	0.0036
c/(kJ/mol)$^{0.5}$ nm^{-3}	0.084 996		

	O−Al	O−H
D_{1ij}/kJ mol^{-1}	90 347.0	21 357.5
β_{1ij}/nm	34.0	55.0
D_{2ij}/kJ mol^{-1}	−20 796.8	−4496.8
β_{2ij}/nm	22.2	29.0
D_{3ijj}/kJ mol^{-1}		65.7
β_{3ij}/nm		77.0
RO$_{3ij}$/nm		0.115

	H−O−H
f_k/10^{-19} J	1.3
θ_0/deg	99.50
g_r/nm^{-1}	9.700
r_m/nm	1.390

(b) Imogolite

	O atom	Si atom	Al atom	H atom
z/e	−1.100	2.200	1.800	0.475
w/10^{-3} kg mol^{-1}	16.00	28.09	26.98	1.01
a/nm	0.1876	0.0810	0.1030	0.0100
b/nm	0.0150	0.0070	0.0080	0.0036
c/(kJ/mol)$^{0.5}$ nm^{-3}	0.084 996			

	O−Si	O−Al	O−H
D_{1ij}/kJ mol^{-1}	12 8540.8	90 347.0	21 357.5
β_{1ij}/nm	39.4	34.0	55.0
D_{2ij}/kJ mol^{-1}	16 835.9	−20 796.8	−4496.8
β_{2ij}/nm	22.2	22.2	29.0
D_{3ijj}/kJ mol^{-1}			65.7
β_{3ij}/nm			77.0
RO$_{3ij}$/nm			0.115

	H−O−H
f_k/10^{-19} J	1.3
θ_0/degree	99.50
g_r/nm^{-1}	9.700
r_m/nm	1.390

TABLE 2: Comparison of Experimental and MD-Simulated Values for Gibbsite Crystal Data

	experimental	simulated
density/g cm^{-3}	2.421	2.403
a/nm	0.8684	0.8799
b/nm	0.5078	0.5066
d spacing/nm	0.9736	0.9785

The two-body terms of potential energy consist of four terms, the Coulomb term, the short-range repulsion term, the van der Waals' term, and the covalent term, which is composed of three terms. The three-body term was used to take into account the sp^3 hybrid orbital of H−O−H. r_{ij} is the distance between the ith and jth atoms, f_0 is a constant, and θ_{jik} is an angle of intra- and intermolecular H−O−H. $\{z, a, b, c, D, \beta, r^*, f_k, \theta_0, g_r, r_m\}$ are parameters to describe the nature of each atom and interactions between atoms. The atomic and interatomic interaction parameters used in this study are shown in Table 1. The parameters with regard to Al−O bonds and O−H bonds were adjusted to reproduce the gibbsite structure. Simulated structural parameters of crystalline gibbsite are compared to experimental values[26] in Table 2. The difference is approximately 1% for all values. The average bond lengths of Al−O and O−H are 0.196 and 0.098 nm, respectively. The parameters of interaction between Si and O were determined to reproduce an average Si−O bond length of 0.162 nm, which was reported for many silicate crystal structures. The bond lengths of OH are close to previously known distances.[27,28]

TABLE 3: Radii of Tubular Gibbsite after the Structures Were Relaxed

N_u	r_{ext}/nm	r_{int}/nm
12		
16		
20	1.79	1.56
24	2.11	1.89

Molecular Dynamics Simulation. The Ewald method was used for the summations of Coulombic interactions. Integration of the equation of atom motions was performed by the velocity Verlet algorithm with a time increment of 0.4 fs. The *NVT* ensemble was employed, where N is the number of atoms in a simulation cell, V is the cell volume, and T is temperature. Temperature was controlled by scaling of atom velocities. Molecular dynamics simulations were carried out at 293 K (MXDORTO[29,30]). The 10 000−50 000-step calculations were performed for the initial relaxation for each system. Subsequent 20 000-step simulations for a single imogolite molecule and tubular gibbsite models and 60 000-step simulations for multiple imogolites model were carried out to obtain ensemble average properties.

Structure Model. The initial structures were generated with a newly developed code that calculates the atom positions of tubular gibbsite and imogolite. As the first step, the procedure makes a ring structure with the number of unit structures of the gibbsite crystal on the circumference of a tube (N_u). Second, the simulation models were made by stacking the rings in the direction of the molecular axis. The structure model of imogolite is based on the model proposed by Cradwick.[1] The compositions of the molecules are $Al(OH)_3$ for the tubular gibbsite molecule and $Al_2(OH)_3SiO_3OH$ for imogolite, respectively.

In this study, six repeating ring structures were involved in one simulation cell for all the systems. The cell sizes (three-dimensional boundary conditions) were 7.20 × 7.20 × 5.04 nm for the model of an isolated imogolite molecule, which were of enough length to be considered as an isolated molecule and to evaluate the Coulomb summation correctly. For the multiple imogolite model, the cell size was 8.80 × 8.80 × 5.04 nm for the system of two molecules in a cell, and 11.0 × 9.00 × 5.04 nm for the three-molecule model.

Models having different N_u were set up; they are N_u = 12, 16, 20, and 24 for the tubular gibbsite and N_u = 10, 12, 13, 14, 15, 16, 17, 20, and 24 for the imogolite, respectively. The snapshots of typical initial structures of the tubular gibbsite and imogolite molecules are shown in Figure 1.

3. Results

Tubular Gibbsite Molecule. Molecular dynamics simulations were carried out to investigate the stability of tubular gibbsite molecules of different diameters of N_u = 12, 16, 20, and 24. The internal and external radius of each structure (r_{int} and r_{ext}, respectively) is shown in Table 3 as an ensemble average, and the snapshots of the models of N_u = 12−24 are shown in Figure 2. The r_{int} and r_{ext} were determined by the average distances of O atoms on the external surface and O atoms on the internal surface, respectively, from the central axis of a molecule.

In models of N_u = 12 and 16, some Al atoms have oxygen coordination numbers of less than 6, where the tubular gibbsite structure was not maintained completely. The relative total

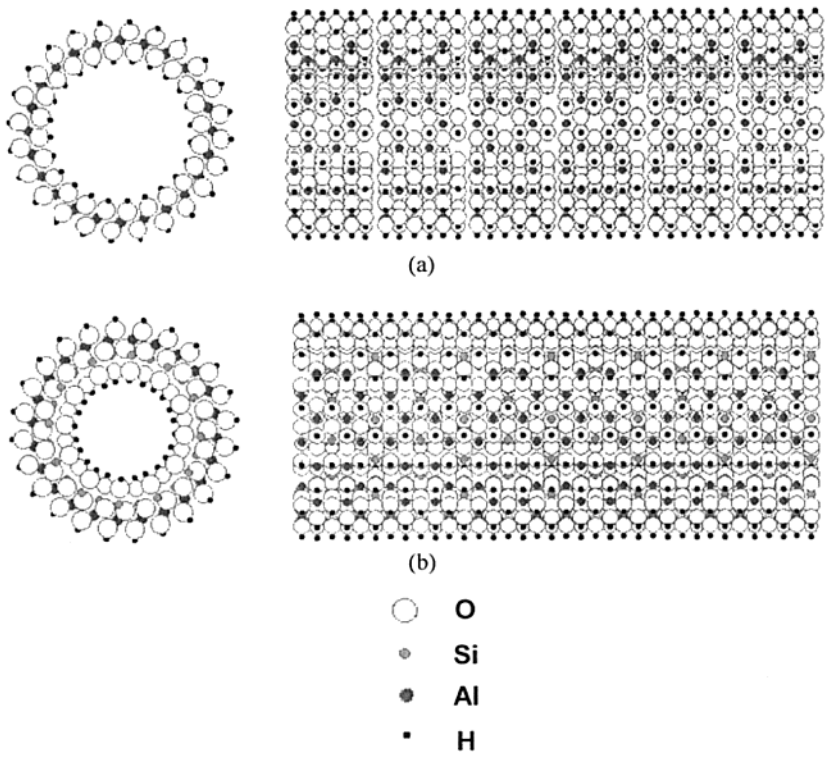

Figure 1. Initial molecular structure models of (a) tubular gibbsite molecule of $N_u = 12$ and (b) imogolite molecule of $N_u = 12$. The left figures in (a) and (b) are viewed from the direction of molecular axis. The right figures are viewed from perpendicular to the molecular axis.

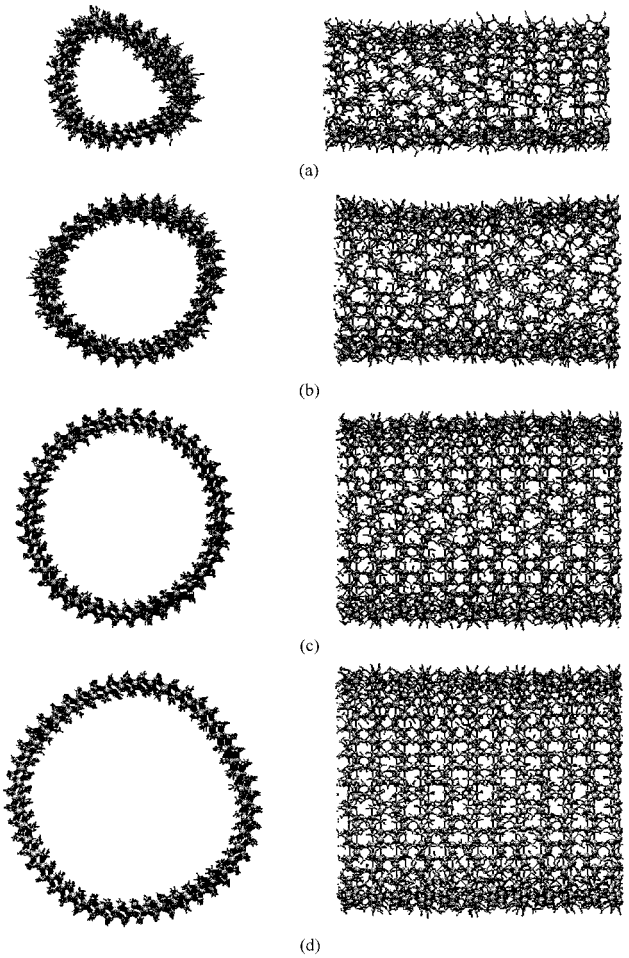

Figure 2. Molecular structures of tubular gibbsite after MD simulations: (a) $N_u = 12$; (b) $N_u = 16$; (c) $N_u = 20$; (d) $N_u = 24$.

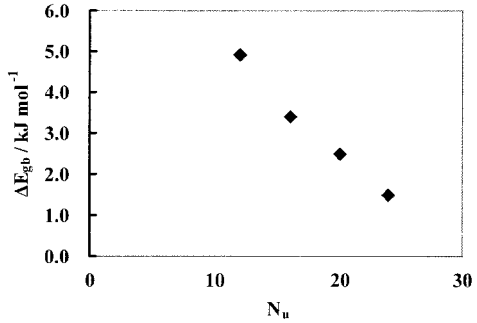

Figure 3. Total energy of tubular gibbsite molecules (ΔE_{gb}), $N_u = 12$, 16, 20, and 24, relative to that of flat gibbsite molecule.

energy (ΔE_{gb}) of the molecules to that of a flat gibbsite molecule is shown in Figure 3. ΔE_{gb} tends to approach zero with the increasing radius of the tube, and ΔE_{gb} is still very large, 1.48 kJ mol^{-1}, even for the structure of $N_u = 24$.

Imogolite Molecule. The pair correlation function of the structure of imogolite with $N_u = 16$ obtained as an average structure at the equilibrium state is in Figure 8. The Si−O, Al−O, and O−H bond lengths are 0.162, 0.194, and 0.096 nm, respectively. These bond lengths are close to those in gibbsite and muscovite structures and to known OH distances as described before.[27,28]

Structural models of imogolite with $N_u = 10$, 12, 13, 14, 15, 16, 17, 20, and 24 were simulated with the molecular dynamics method to obtain the structural details and energetics. The internal and external radius of each model (r_{int} and r_{ext}, respectively) are shown in Table 4, and the snapshots of the model of $N_u = 12$ at the equilibrium state are shown in Figure 4. r_{int} and r_{ext} were determined by the average distances of O atoms on the external surface and O atoms of SiOH's from the center of the tube axis, respectively.

In imogolite molecules, all the 6-coordinated Al and 4-coordinated Si structures were stably maintained even if they had

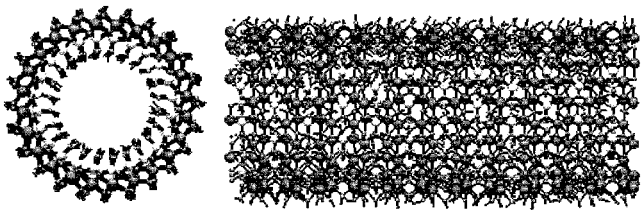

Figure 4. Imogolite molecular structure of $N_u = 12$ after MD simulation was carried out.

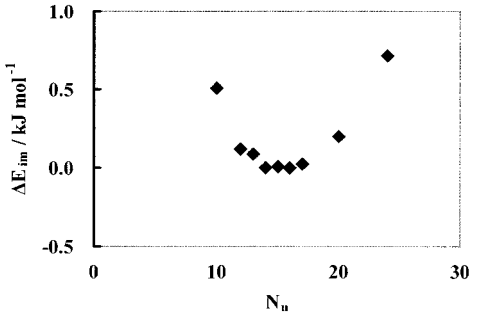

Figure 5. Total energy of imogolite (ΔE_{im}), $N_u = 10$, 12, 13, 14, 15, 16, 17, 20, and 24, relative to the minimum energy of $N_u = 16$.

TABLE 4: Radii of Imogolite Molecule after the Structures Were Relaxed

N_u	r_{ext}/nm	r_{int}/nm
10	0.95	0.51
12	1.09	0.65
14	1.25	0.81
15	1.33	0.89
16	1.43	0.99
20	1.69	1.25
24	2.03	1.60

an extremely small radius as $N_u = 10$. The relative total energy that was shown as a difference (ΔE_{im}) from the energy of $N_u = 16$, which has a minimum total energy throughout imogolite molecules, was plotted in Figure 5. The ΔE_{im} of $N_u = 14$ and 15 are almost the same as that of $N_u = 16$. R_{ext}'s are from 1.25 to 1.43 nm.

Molecular Dynamics Simulation of Multiple Imogolite Molecules. The molecular diameters of the natural and synthetic imogolite were reported experimentally as 2.1−2.8 nm, which should not be compared with the diameters directly calculated from R_{ext}'s because of the different means of measurement. The center-to-center distances of $N_u = 14-16$ imogolite were investigated as an ensemble average by using the multiple imogolite models to make the proper comparison. The center of each imogolite molecule was calculated from the positions of Al atoms. Two models were prepared: one had two imogolite molecules in a simulation cell (model A), and the other had three imogolite molecules in a cell (model B). The initial structures were set to be imogolite molecules placed in parallel, and *NVT*-MD simulations were performed. We needed approximately 100 000 steps calculations to obtain relaxed structures. Afterward, 60 000-step simulations were carried out to obtain ensemble average properties. The snapshots of equilibrated structures are shown in Figure 6.

It is observed that the imogolite molecules stably stick on each other through hydrogen bonds that are formed between surfaces of imogolite tubes. The center-to-center distances of imogolite in the multiple models were shown in Table 5. The values obtained from the three-molecule model were slightly short compared with corresponding values in the two-molecule model because of deformation of the center imogolite.

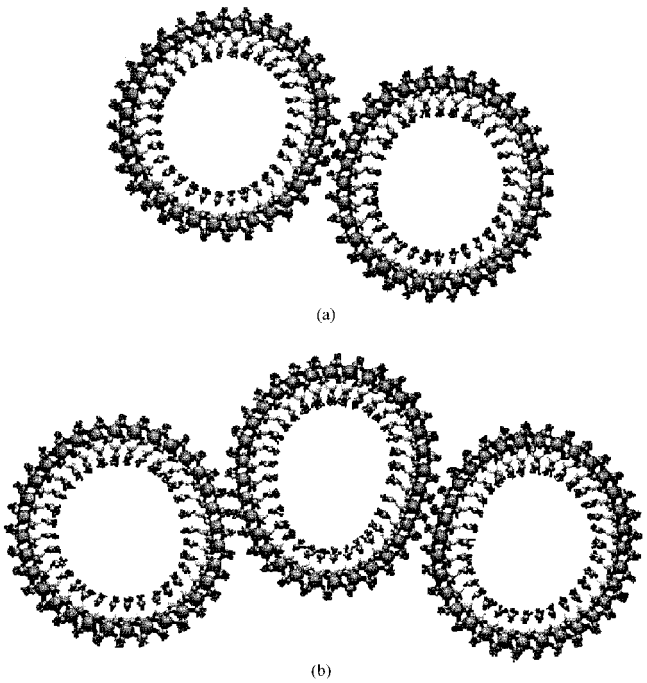

Figure 6. Molecular structures of multiple imogolite model viewed from the direction of molecular axis: (a) the two-imogolite model; (b) the three-imogolite model.

TABLE 5: Center-to-Center Distances Simulated by the Multiple Imogolite Models, d_A, for the Model A (Two Molecules), and d_B, for the Model B (Three Molecules) as an Average of the Two Center-to-Center Distances

N_u	d_A/nm	d_B/nm
14	2.67	2.62
15	2.79	2.76
16	2.93	2.89

Vibrational Spectra of Imogolite Molecule. The vibrational spectra of imogolite with $N_u = 16$ was simulated by performing Fourier transformation of the velocity autocorrelation function of atoms, which can be compared with neutron inelastic scattering spectra. O atoms in the gibbsite sheet (denoted as O_{AlOAl}) and in Si−OH (O_{SiOH}) were treated separately, which enables us to identify the spectra regarding O atoms in detail. Similarly, H atoms bonding with O_{AlOAl} (H_{AlOAl}) and with O_{SiOH} (H_{SiOH}) were treated separately. The vibrational spectra of these atomic species and IR spectra of the synthetic imogolite (private communication from M. Suzuki) are shown in Figure 7.

Three bands observed near 1000 cm^{-1}, i.e., 937, 972, and 1028 cm^{-1}, were assigned to the Si−O stretching vibration. The intensive bands centered at 937 and 972 cm^{-1} were identified as an Si−O_{SiOH} stretching vibration because they were observed simultaneously with regard to the spectra of Si and O_{SiOH}.

The band centered at 1028 cm^{-1} was shown as a relatively large peak in the spectra of O_{AlOAl}, which can be considered as an Si−O_{AlOAl} stretching vibration because the corresponding band at 1028 cm^{-1} was observed in the Si spectra. This stretching motion seemed to influence the motion of O_{SiOH} since the small peak at the same wavenumber was observed in the spectra.

The O_{SiOH}−H_{SiOH} stretching has a sharp band centered at 3729 cm^{-1}. On the other hand, there are several bands for the O_{AlOH}−H_{AlOH} bond in a wide range of wavenumbers.

4. Discussion

Comparison of Vibrational Spectra. In the process of analyzing vibrational spectra, we will not go further to try to

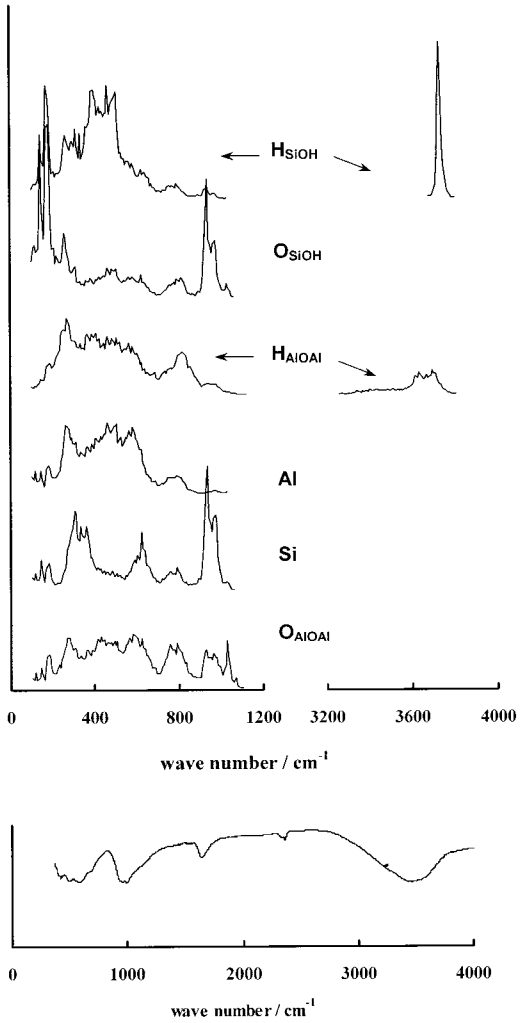

Figure 7. Vibrational spectra of each atom species in the imogolite simulated by MD (upper) and IR spectra of synthetic imogolite (lower).

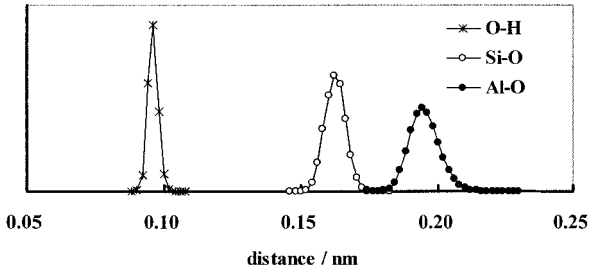

Figure 8. Pair correlation functions of the O−H, Si−O, and Al−O for a imogolite molecule with $N_u = 16$.

interpret all peaks because vibration that results from each atom and that from a whole molecule were not separated enough in this work.

However, Si−O vibrational spectra obtained near 1000 cm^{-1} agree well with the results of the IR spectra, so that we consider the interatomic potential model of Si−O was determined properly. The peaks regarding Al−O bonds were not identified because of the broad and complex bands. The O−H stretching vibration was observed at a higher wavenumber compared to IR spectra. In this calculation, the imogolite molecule was simulated as an isolated molecule in a vacuum. The difference can be explained by an influence of the adsorbed water molecules on the molecular surface that interact with H_{AlOAl} and H_{SiOH} of imogolite. This interaction would make O−H bonds weaker and cause the shift of the peak toward lower wavenumbers.

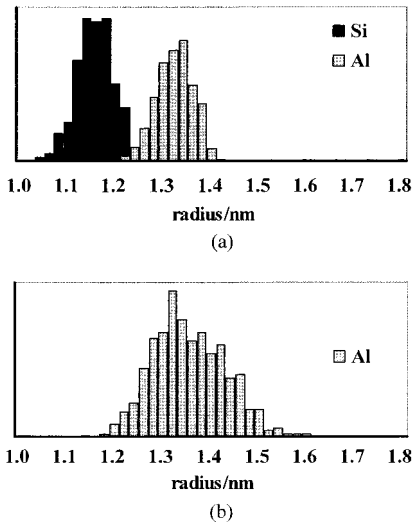

Figure 9. Distribution of the radius (a) defined by the distance of Si and Al atoms from the central axis of the imogolite molecule of $N_u = 16$ and (b) defined by the distance of Al atoms from the central axis of the tubular gibbsite of $N_u = 16$.

Stability of Tubular Structure. The structural stability of tubular molecules was investigated by calculating the distribution of the radius of tubes which fluctuated with time. The positions of O atoms in tubular gibbsite with $N_u = 16$ and the positions of Si and Al atoms in imogolite of $N_u = 16$ as a function of the distance from the molecular axis (radii of the tubes) are shown in Figure 9. The tubular gibbsite structure could be concluded rather loosely since the distribution of the radius is broad. For imogolite, the width of the radius distribution is less than 10%. The tetrahedra bonded in the vicinity of vacant octahedral sites of the gibbsite structure are considered to stabilize the tubular structure.

The tubular gibbsite molecule with relatively small radius ($N_u = 12$ and 16) could not retain its 6-coordinated Al structure partially, which led to the deformed tubular structure. The total energy of tubular gibbsite decreases with the increasing radius of the tube and approaches slowly the total energy of the flat gibbsite molecule without showing energy minima. This result shows that the gibbsite structure prefers the flat state to the tubular states. Unlike the tubular gibbsite, the imogolite tubular structure is structurally stable even if it has a small radius and has the energy minimums at $N_u = 14-16$.

In an attempt to explain how the total energy of imogolite has the minimum, the atom potential energy of each atomic species and the pair correlation functions of O−O, Si−O, and Al−O of imogolite with $N_u = 10-24$ were examined. The distributions of atom potential energies and the pair correlation functions are shown in Figures 10 and 11. The O atoms of imogolite are classified into three groups: the O atoms in Al−OH−Al on the external surface (group 1), O atoms in Al−O−Si (group 2), and O atoms in Si−OH (group 3). The lowest oxygen potential energy is of group 2. Group 3 was shown as one peak with the highest potential energy, and group 1 corresponded to one or two species whose potential energies are observed between those of groups 2 and 3. The oxygen potential energy for all the groups decreases with the increasing radius of the tube. For distribution of O−O distances of both tetrahedra and octahedra, the components corresponding to the shortest O−O distances disappeared with increasing N_u. This elongation of the shortest O−O should be very likely the cause

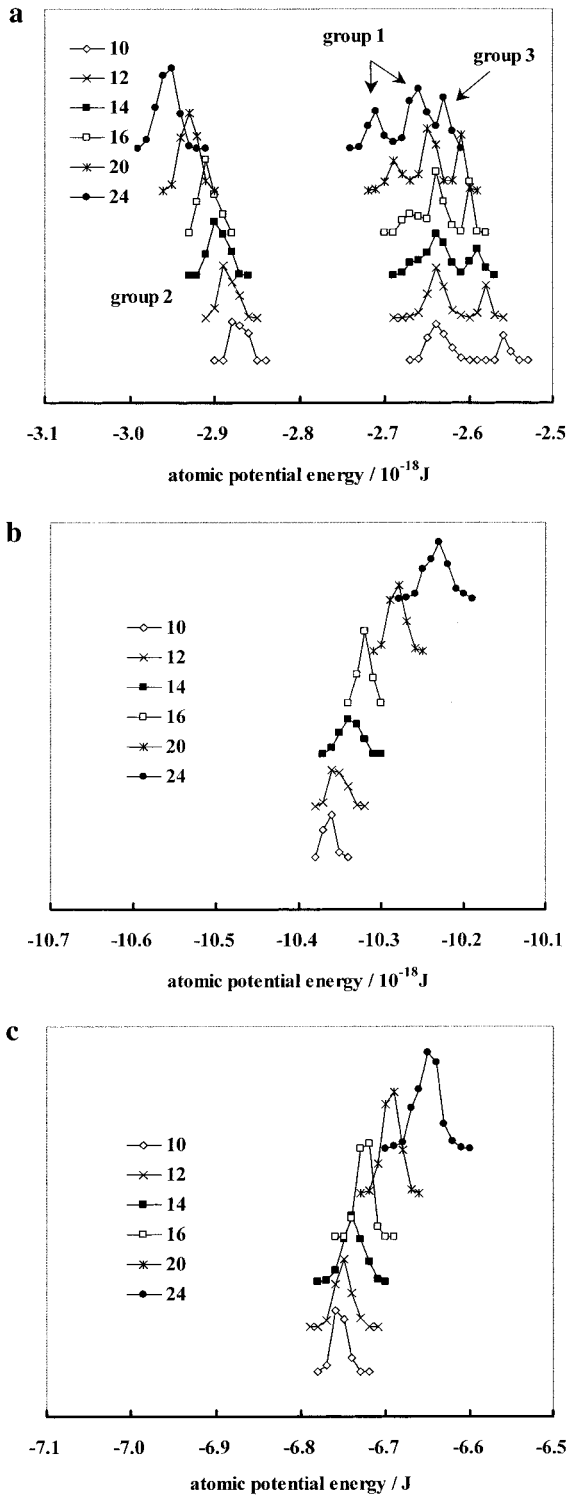

Figure 10. Atomic potential energies of imogolite molecules corresponding to $N_u = 10$, 12, 14, 16, 20, and 24, (a) for O atoms, (b) for Si atoms, and (c) for Al atoms.

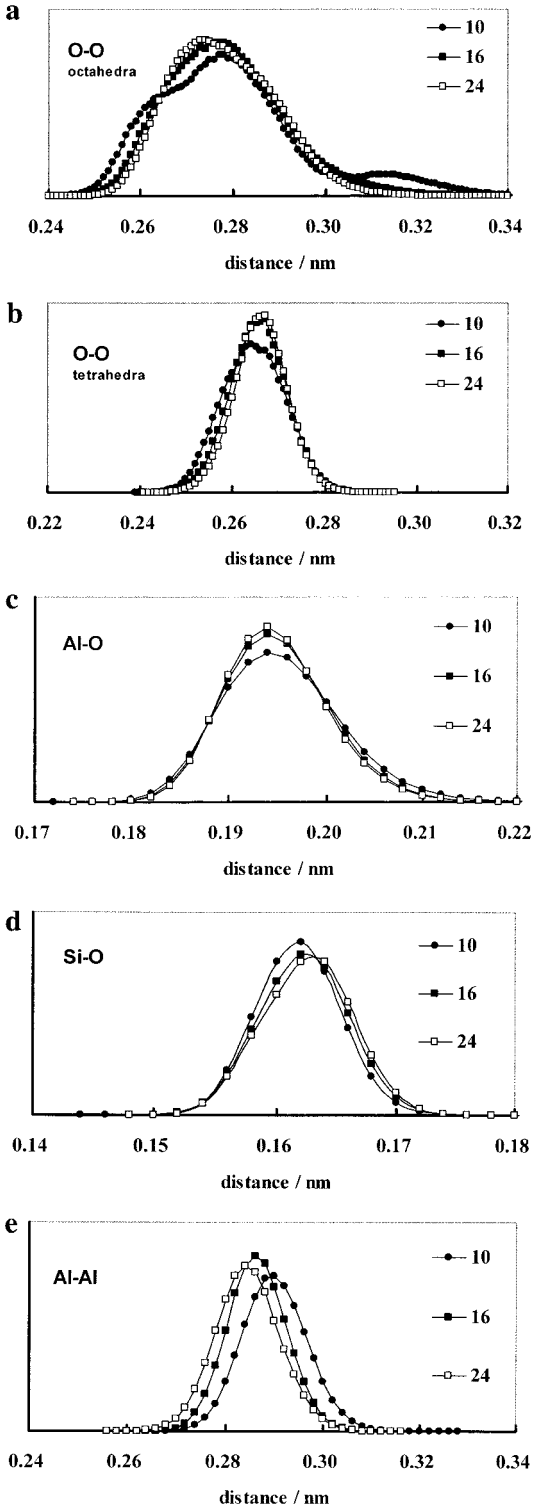

Figure 11. Pair correlation functions for imogolites with $N_u = 10$, 16, and 24: (a) O−O distance in the coordination polyhedra of octahedral Al, (b) O−O distance in the coordination polyhedra of tetrahedral Si, (c) octahedral Al−O distance, (d) tetrahedral Si−O distance, and (e) Al−Al distance between edge shared octahedral sites.

of the decrease of the potential energy. The atom potential energies of both Al and Si increase with increasing N_u; however, this tendency could be explained by different phenomena. It was shown that the SiO_4 tetrahedra became larger with N_u since the pair correlation function of Si−O shifted toward a longer distance. The increase of the potential energy of Si should stem from the Si−O elongation. On the other hand, the pair correlation function of Al−O showed a small change compared to Si−O, indicating the deformation of octahedra was not as large as that of tetrahedra. Instead, the Al−Al distribution changed apparently, shifting toward a short distribution from 0.290 nm at $N_u = 10$ to 0.284 nm at $N_u = 24$. The possible explanation for the potential energy rising of the Al atom may be the shortening of the Al−Al distance of edge-shared octahedra resulting from enlargement of the tube radius. It is concluded that the minimum of the total energy simulated for imogolite molecules that have $N_u = 14-16$ are produced as a consequence of the balance of atomic potential energies

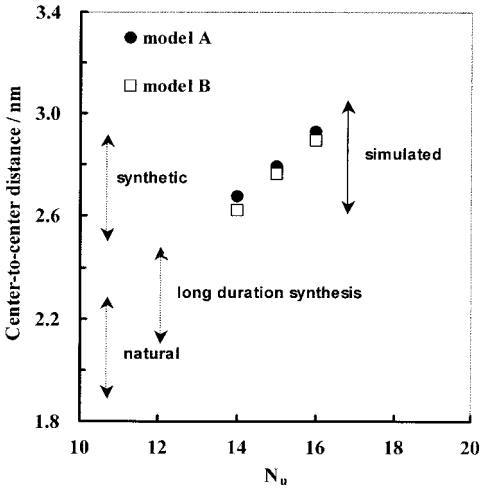

Figure 12. Simulated center-to-center distance of imogolites as a function of N_u. Model A means the system contains two tubes, and model B three tubes. The ranges of the reported diameters of natural and synthetic imogolite are also shown.

described above. Furthermore, the instability observed upon large N_u could stem from both the Si−O enlargement and the Al−Al shortening.

Diameter of Imogolite Molecule. The ranges that are shown by arrows as "natural" and "synthetic" in Figure 12 are experimentally observed diameters derived from center-to-center distances between tubes, that is, from 2.1 to 2.3 nm for the natural imogolite and from 2.5 to 2.8 nm for the synthetic imogolite. It has not been explained experimentally how the difference of diameters between synthetic and natural imogolite occurred. The range of simulated center-to-center distances near the energy minimum, from 2.62 nm ($N_u = 14$) to 2.89 nm ($N_u = 16$), is also shown, which is close to the value of the synthetic imogolite.

The simulated diameters should not be directly compared with the experimentally observed diameters because the simulations were carried out in extreme conditions, in which two and three imogolites are in absolute vacuum and there are no water molecules in the system. Furthermore, it should be emphasized that the models used in this study were perfect molecules, which means the models have no defects. As described before, the diameter of imogolite synthesized at room temperature in the long duration was closer to that of natural molecules.[6] It might be possible that the structural defects influence the diameter. The interatomic potential model parameters also have some uncertainty. The model parameters can be improved by carrying out large-scale molecular orbital calculations. The study of the effect of structural defects and the refinement of potential parameters are future subjects.

5. Summary

The interatomic potential model was derived to simulate tubular imogolite and gibbsite molecules, and the model of imogolite that is based on the model proposed by Cradwick et al.[1] was simulated with the molecular dynamics method. The pair correlation function shows that bond lengths of this structure correspond with experimental data reported before. The vibrational spectra of the Si−O bond simulated were also similar to experimental infrared spectra.

The stability of the tubular structure of imogolite was evaluated, compared with the model of the tubular gibbsite molecule because they have part of the structure in common: an octahedral layer. The dependency of the tube stability upon tube radii was also evaluated. The potential energy of tubular gibbsite decreases with the increasing radius of the tube and approaches the potential energy of a flat gibbsite molecule. This result shows that the gibbsite structure prefers the planar state to the tubular states. On the contrary, the potential energy of imogolite shows the minimum at $N_u = 14-16$. The stability of the imogolite structure was examined by using the results of the molecular dynamics simulation. From the distribution of the radius, it is shown that the tubular structure of imogolite is more stable than that of the tubular gibbsite. The tetrahedra bonded in the vicinity of the vacant octahedral sites of the gibbsite structure are considered to stabilize the tubular structure.

The structural contribution to the stability of the imogolite tube was examined by the pair correlation functions and the atomic total potential energy. The enlargement of SiO_4 tetrahedra and the shortening of Al−Al distance with increasing N_u are shown. As a result of these structural changes, the atomic potential energies of Al and Si were raised, whereas the atomic potential energy of oxygen decreased with increasing N_u. It is concluded that the total energy minimum is formed as a consequence of the balance of atomic potential energies of Si, Al, and O.

Acknowledgment. We cordially thank Dr. M. Suzuki (National Institute of Advanced Industrial Science and Technology) for his data and for helpful discussions.

References and Notes

(1) Cradwick, P. D. G.; Farmer, V. C.; Russell, J. D.; Masson, C. R.; Wada, K.; Yoshinaga, N. *Nature Phys. Sci.* **1972**, *240*, 187.

(2) Farmer, V. C.; Fraser, A. R.; Tait, J. M. *J. Chem. Soc., Chem. Commun.* **1977**, 462.

(3) Farmer, V. C.; Fraser, A. R. *Int. Clay Conf.* **1978**.

(4) Wada, S.-I.; Eto, A.; Wada, K. *J. Soil Sci.* **1979**, *30*, 347.

(5) Wada, S.-I.; Wada, K. *Clays Clay Miner.* **1982**, *30*, 2, 123.

(6) Wada, S.-I. *Clays Clay Miner.* **1987**, *35*, 5, 379.

(7) Bursill, L. A.; Peng, J. L.; Bourgeois, L. N. *Philos. Mag. A* **2000**, *80*, 1, 105.

(8) Johnson, I. D.; Werpy, T. A.; Pinnavaia T. J. *J. Am. Chem. Soc.* **1988**, *110*, 25, 8545.

(9) Johnson, L. M.; Pinnavaia T. J. *Langmuir* **1990**, *6*, 2, 307.

(10) Johnson, L. M.; Pinnavaia T. J. *Langmuir* **1991**, *7*, 11, 2636.

(11) Imamura, S.; Hayashi, Y.; Kajiwara, K.; Hoshino, H.; Kaito, C. *Ind. Eng. Chem. Res.* **1993**, *32*, 4, 600.

(12) Imamura, S.; Kokubu, T.; Yamashita, T.; Okamoto, Y.; Kajiwara, K. *J. Catal.* **1996**, *160*, 1, 137.

(13) Chang, F.-R. C.; Skipper, N. T.; Sposito, G. *Langmuir* **1995**, *11*, 2734.

(14) Park, S.; Fitch, A.; Wang, Y. *J. Phys. Chem. B* **1997**, *101*, 4889.

(15) Kutter, S.; Hansen, J.-P.; Sprik, M.; Boek, E. *J. Chem. Phys.* **2000**, *112*, 1, 311.

(16) Ghassemzadeh, J.; Xu, L.; Tsotsis, T.; Sahimi, M. *J. Phys. Chem. B* **2000**, *104*, 3892.

(17) Williams, S. J.; Coveney, P. V.; Jones, W. *Mol. Simul.* **1999**, *21*, 183.

(18) Warne, M. R.; Allan, N. L.; Cosgrove, T. *Phys. Chem. Chem. Phys.* **2000**, *2*, 3663.

(19) Kawamura, K.; Ichikawa, Y.; Nakano, M.; Kitayama, K.; Kawamura, H. *Eng. Geol.* **1999**, *54*, 75.

(20) Ichikawa, Y.; Kawamura, K.; Nakano, M.; Kitayama, K.; Kawamura, H. *Eng. Geol.* **1999**, *54*, 21.

(21) Kawamura, K.; Ichikawa, Y.; Nakano, M.; Kitayama, K.; Kawamura, H. *Mater. Res. Soc. Proc.* **1998**, *506*, 359.

(22) Pohl, P. I.; Smith, D. M. *Adv. Porous Mater.* **1995**, 27.

(23) Hoshino, H.; Urakawa, H.; Kajiwara, K.; Donkai, N. *Polym. Bull.* **1996**, *36*, 2, 257.

(24) Pohl, P. I.; Faulon, J.-L.; Smith, D. M. *Langmuir* **1996**, *12*, 18, 4463.

(25) Kumagai, N.; Kawamura, K.; Yokokawa, T. *Mol. Simul.* **1994**, 12, 177.
(26) Saalfeld, H.; Wedde, M. *Z. Krystallogr*. **1974**, *139*, 129.
(27) Guggenheim, S.; Chang, Y.-H.; Koster van Groos, A. F. *Am. Miner.* **1987**, *72*, 537.
(28) Wang, S.-L.; Johnston, C. T. *Am. Miner*. **2000**, *85*, 739.
(29) Kawamura, K. JCPE #026, 1992−2000.
(30) Kawamura, K. In *Molecular Dynamics Simulations*; Yonezawa, F., Ed.; Springer-Verlag: Berlin, 1992.